# Intensity phase coherence in three-mode Fabry-Pérot lasers

Ba An Nguyen and Paul Mandel
*Optique Nonlinéaire Théorique, Université Libre de Bruxelles, Campus Plaine C.P. 231, B-1050 Bruxelles, Belgium*
(Received 22 February 1996)

We study analytically the intensity phase coherence in a three-mode Fabry-Pérot laser. We consider in detail the case of a central mode with maximum gain and two side modes with smaller but equal gains. This laser is characterized by three relaxation oscillation frequencies $\Omega_R''>\Omega_{L1}''>\Omega_{L2}''$. In the framework of a linearized theory, the laser dynamics is, respectively, inphased and perfectly antiphased at $\Omega_R''$ and $\Omega_{L2}''$, irrespective of the modal gains. At $\Omega_{L1}''$ the antiphase is only partial if the side mode gains are smaller than the central mode gain. Analytic gain- and pump-dependent relations between the three frequencies and between the heights of the peaks in the power spectra at these frequencies are established. We also derive universal relations between the peaks of the power spectra of the modal and the total intensities at the same frequencies that do not involve any parameter at all. [S1050-2947(96)00908-0]

PACS number(s): 42.65.Sf

## I. INTRODUCTION

Phase coherence is a figure of merit for the spontaneous self-organization of nonlinear systems composed of globally coupled components. The dynamics of individual components is complex in general but they may be correlated in phase so that the dynamics of the whole system is much simpler. Such a property is known in laser physics as antiphase dynamics (AD). It has been recognized for the self-pulsing state [1–4], in externally modulated lasers [5,6], in the noise spectrum at steady state [7], in the transient relaxation to steady state [8–10], in the chaotic regime [11,12], and in the routes to chaos [13]. In this paper we consider multimode Fabry-Pérot lasers in which the mode-mode coupling is mediated by spatial hole burning of the population inversion. AD is most pronounced when the mode-mode competition is maximum, namely, when the modal gains are close to each other. Thus most theoretical studies have been restricted to the reference model derived in [14] in which all gains are equal. One of the simplest signatures of AD is the fact that the power spectrum of the total intensity has *fewer* peaks than the power spectrum of the modal intensities. This cancellation signs a coherence effect. This is surprising since we deal only with lasers that are described by the Tang, Statz, and deMars rate equations [15] that couple the modal intensities to the population inversion. We distinguish between perfect AD, where a peak at one of the low frequencies completely disappears in the power spectrum of the total intensity, and partial AD, where only a reduction in the peak height of the total intensity power spectrum is observed. From a symmetry point of view, the perfect AD obtained in the reference model is due to the equality of the modal gains. In practice, however, the modal gains are not exactly equal. Then the phases of the time-dependent modal intensities do not cancel out completely. This results in a partial AD. Such a signature of AD has recently been analyzed in [16].

Another influence of the gain difference is related to the internal relaxation oscillation frequencies. When all gains are equal, there are only two relaxation oscillation frequencies and their ratio varies in the narrow interval $[\sqrt{2N-1},\sqrt{2N+1}]$ where $N$ is the number of modes [17]. Of interest are mode numbers for which there is an integer in that range because we may then expect resonances to appear if an external modulation is applied to the laser. However, a difference in gains will change this situation drastically by increasing the number of relaxation frequencies [18] and possibly inducing new relations that may favor other resonant responses to an external modulation. For these reasons, we present a study of the three-mode Fabry-Pérot laser in the frequently occurring situation of a symmetric pattern: one central mode and two side modes with smaller but equal gains.

This paper is organized as follows. In Sec. II we solve the Tang, Statz, and deMars (TSD) equations in steady state. We determine the necessary and sufficient conditions for the laser to operate on $N$ modes. A linear stability analysis is performed in Sec. III in which we establish the relation between the peak heights in the power spectra of the modal and total intensities for the same frequency as well as relations between the three frequencies. The degree of intensity phase coherence at each frequency is obtained analytically and compared with the numerical evaluation. Conclusions are presented in the final section.

## II. $N$-MODE REGIME: NECESSARY AND SUFFICIENT CONDITIONS

The multimode Fabry-Pérot laser can be described by the TSD equations [15]

$$\frac{\partial I_p}{\partial t}=k\left[\gamma_p\left(D-\frac{D_p}{2}\right)-1\right]I_p, \tag{1}$$

$$\frac{\partial D_p}{\partial t}=\gamma_p I_p D-D_p\left(1+\sum_q \gamma_q I_q\right), \tag{2}$$

$$\frac{\partial D}{\partial t}=w-D-\sum_q \left(D-\frac{D_p}{2}\right)\gamma_q I_q, \tag{3}$$

where $p$ and $q=1,2,\ldots,N$, the modal intensities are $I_p$ while $D_p$ and $D$ are defined through the population inversion $D(x,t)$ as

 

$$D_p=\frac{2}{L}\int_0^L \overline{D}(x,t)\cos(2px)dx \quad \text{and} \quad D=\frac{1}{L}\int_0^L \overline{D}(x,t)dx,$$

with $L$ being the cavity length. In (1)–(3) the time $t$ is time measured in units of the population inversion decay time. The modes are characterized by their gain. The parameter $\gamma_p$ is the gain of mode $p$ divided by the gain of the first mode. Hence $\gamma_1\equiv 1$. The pump rate $w$ is normalized in such a way that the first mode starts to oscillate at $w=1$. The inverse photon lifetime $k$ is assumed to be mode independent but the modal gains $\gamma_p$ are mode dependent.

Let us denote by $I_p^s$, $D_p^s$, and $D^s$ the steady-state solution that does not depend on $k$ and satisfies the equations

$$\left[\gamma_p\left(D^s-\frac{D_p^s}{2}\right)-1\right]I_p^s=0, \tag{4}$$

$$\gamma_p I_p^s D^s=D_p^s\left(1+\sum_q \gamma_q I_q^s\right), \tag{5}$$

$$w=D^s+\sum_q \left(D^s-\frac{D_p^s}{2}\right)\gamma_q I_q^s. \tag{6}$$

Making use of the fact that $I_p^s>0$ for $p\leqslant N$, we get from (4) and (5)

$$D_p^s=2\left(D^s-\frac{1}{\gamma_p}\right), \tag{7}$$

$$I_p^s=\frac{D^s-1/\gamma_p}{\gamma_p[S_1-(N-\frac{1}{2})D^s]}, \quad S_1=\sum_{q=1}^{N}\frac{1}{\gamma_q}. \tag{8}$$

Since $D^s$ is positive, (5) is satisfied if and only if $D_p^s>0$ or, on account of (7)

$$D^s>\frac{1}{\gamma_p}. \tag{9}$$

Taking (9) into account in (8), the positivity of $I_p$ requires

$$\frac{S_1}{N-\frac{1}{2}}>D^s. \tag{10}$$

The steady-state population inversion $D^s$ satisfies Eq. (6), which can be written as

$$w=D^s+\frac{D^sS_1-S_2}{S_1-(N-\frac{1}{2})D^s}, \quad S_2=\sum_{q=1}^{N}\frac{1}{\gamma_q^2}. \tag{11}$$

Equation (11) is quadratic in $D^s$. However, only one of the two solutions may satisfy condition (10),

$$D^s=\frac{S_1}{N-\frac{1}{2}}+\frac{w}{2}-\frac{\sqrt{\Delta}}{2N-1}, \tag{12}$$

$$\Delta=(N-\tfrac{1}{2})^2w^2+4[S_1^2-(N-\tfrac{1}{2})S_2]>0. \tag{13}$$

Requiring that the solution (12) satisfy (10) leads to the inequality $\sqrt{\Delta}>(N-1/2)w$ or, equivalently,

$$S_1^2-(N-\tfrac{1}{2})S_2>0. \tag{14}$$

If the condition (14) is satisfied, $\Delta>0$ for any $w$ guaranteeing that $D^s$ is real and positive. Condition (14) is the necessary condition on the gain in order that the laser operate on $N$ modes. To be sufficient, the inequality (9) must be fulfilled as well. This imposes the constraint on the pump,

$$w>w_N=\frac{1}{\gamma_{\min}}+\frac{S_1-S_2\gamma_{\min}}{S_1\gamma_{\min}-N+\frac{1}{2}}, \tag{15}$$

where $\gamma_{\min}$ is the smallest among the gains and $w_N$ is referred to as the $N$-mode threshold pump. It follows from (4), (6), and (9) that $w_N$ is always greater than $1/\gamma_{\min}$. On the other hand, from (9) and (10) we have $\gamma_{\min}>(N-1/2)/S_1$. Therefore $\gamma_{\min}\leqslant S_1/S_2$. Combining these relations yields the necessary condition on the gain $\gamma_{\min}$,

$$\frac{N-\frac{1}{2}}{S_1}<\gamma_{\min}\leqslant\frac{S_1}{S_2}. \tag{16}$$

Since the condition (14) is automatically satisfied if the condition (16) is satisfied, the necessary and sufficient conditions for the laser to operate on $N$ modes are (15) and (16). In particular, if all gains are equal then all the modes lase simultaneously provided only that $w>w_N=1$. On the contrary, if the gains are different an $N$-mode operation requires that both (15) and (16) be fulfilled, which constrains both the gains and the pump. We illustrate this point for $N=2$ and 3.

### A. Two-mode operation

The condition (15) yields

$$w_2=\frac{1}{\gamma_2}+\frac{2(1-\gamma_2)}{2\gamma_2-1}, \tag{17}$$

while (16) gives

$$\tfrac{1}{2}<\gamma_2\leqslant 1. \tag{18}$$

The relative gain of mode 2 should exceed 1/2 in order that mode 2 can join mode 1 to operate in a two-mode regime.

### B. Three-mode operation

We assume $\gamma_2\geqslant\gamma_3$ and that the laser is operating in a two-mode regime, i.e., $\gamma_2$ is in the interval defined by (18). The condition (16) becomes

$$\frac{3\gamma_2}{2(\gamma_2+1)}<\gamma_3\leqslant\frac{\gamma_2(\gamma_2+1)}{\gamma_2^2+1}.$$

Yet, because $\gamma_2(\gamma_2+1)/(\gamma_2^2+1)\geqslant\gamma_2$ for $\gamma_2\leqslant 1$, the actual domain for $\gamma_3$ is

$$\frac{3\gamma_2}{2(\gamma_2+1)}<\gamma_3\leqslant\gamma_2. \tag{19}$$

The domain of three-mode operation in the $(\gamma_2,\gamma_3)$ plane is shown in Fig. 1. In particular, if $\gamma_2=1$ the smallest value

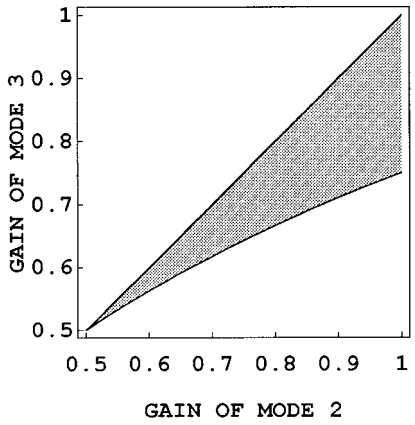


FIG. 1. Domain for three-mode operation in the $(\gamma_2,\gamma_3)$ parameter plane. The lower bound is excluded.

required for $\gamma_3$ to set in a three-mode operation is $\gamma_3=\frac{3}{4}$. From the condition (15) we obtain the pump threshold for three-mode operation,

$$w_3=\frac{1}{\gamma_3}+\frac{2[\gamma_2(\gamma_2+1)-\gamma_3(\gamma_2^2+1)]}{\gamma_2[2\gamma_3(\gamma_2+1)-3\gamma_2]}. \tag{20}$$

## III. INTENSITY PHASE COHERENCE

A basic property of solid-state lasers for our analysis is the fact that $k$ is large, ranging from about $10^4$ for Nd:YAG (YAG denotes yttrium-aluminum-garnet) lasers to about $10^6$ for LNP lasers. Following the method proposed in [14], we introduce $\delta=1/\sqrt{k}$ as a small parameter, scale the time as $\tau=t/\delta$ [14], and introduce the following decomposition:

$$I_p=I_p^s+\mathfrak{T}_p,$$

$$D_p=D_p^s+\delta\mathfrak{D}_p,$$

$$D=D^s=\delta\mathfrak{D},$$

with $\mathfrak{T}_p$, $\delta\mathfrak{D}_p$, and $\delta\mathfrak{D}$ being the deviations from the corresponding steady-state values. We expand to leading order in $\delta$ the equations for the deviations and we linearize them. The result is

$$\frac{\partial\mathfrak{T}_p}{\partial\tau}=\gamma_p\left(\mathfrak{D}-\frac{\mathfrak{D}_p}{2}\right)I_p^s,$$

$$\frac{\partial\mathfrak{D}_p}{\partial\tau}=\gamma_p\mathfrak{T}_pD^s-D_p^s\sum_q\ \gamma_q\mathfrak{T}_q+\delta\left[\gamma_p\mathfrak{D}I_p^s-\mathfrak{D}_p\left(1+\sum_q\ \gamma_qI_q^s\right)\right],$$

$$\frac{\partial\mathfrak{D}}{\partial\tau}=-\sum_q\ \mathfrak{T}_q-\delta\left[\mathfrak{D}+\sum_q\ \gamma_q\left(\mathfrak{D}-\frac{\mathfrak{D}_p}{2}\right)I_q^s\right].$$

The linearity of these equations means that we can seek solutions of the form $(\mathfrak{T}_p,\mathfrak{D}_p,\mathfrak{D})=(\mathbb{I}_p,\mathbb{D}_p,\mathcal{D})\exp(\lambda t)$. Let us define a state vector

$$z=\{\mathcal{D},\mathcal{S},\mathcal{N},\mathbb{I}_2,\mathbb{D}_2,\mathbb{I}_3,\mathbb{D}_3\}, \tag{21}$$

where $\mathcal{S}=\Sigma_q\ \mathbb{I}_q$ and $\mathcal{N}=\Sigma_q\mathbb{D}_q$. Such a $z$ representation is helpful because it allows one to follow at the same time both the modal and the total intensities and population gratings. In this representation the characteristic equation for $\lambda$ is

$$\det\begin{vmatrix}
\lambda+\delta U & 1 & -\delta A_1 & 0 & \delta(A_1-A_2) & 0 & \delta(A_1-A_3)\\
-Y & \lambda & A_1 & 0 & A_2-A_1 & 0 & A_3-A_1\\
-\delta Y & C_1 & \lambda+\delta U & C_2-C_1 & 0 & C_3-C_1 & 0\\
-2A_2 & 0 & 0 & \lambda & A_2 & 0 & 0\\
-2\delta A_2 & H_{12} & 0 & K_{21} & \lambda+\delta U & H_{32}-H_{12} & 0\\
-2A_3 & 0 & 0 & 0 & 0 & \lambda & A_3\\
-2\delta A_3 & H_{13} & 0 & H_{23}-H_{13} & 0 & K_{31} & \lambda+\delta U
\end{vmatrix}=0,$$

with the notations

$$A_p=\gamma_pI_p^s/2,\quad C_p=\gamma_p(5D^s-2S_1),\quad H_{pq}=\gamma_pD_q^s,$$

$$K_{pq}=H_{pp}-H_{qp}-\gamma_pD^s,\quad Y=\sum_q\ \gamma_qI_q^s,\quad U=1+Y.$$

Up to first order in $\delta$ we write $\lambda=\omega-\delta\Gamma$ and determine $\omega$ as roots of the equation

$$\omega f(\omega^2)=0,\quad f(\omega^2)=\omega^6+\alpha_2\omega^4+\alpha_1\omega^2+\alpha_0, \tag{22}$$

and $\Gamma$ as functions of these roots,

$$\Gamma=\frac{4U\omega^6+\beta_2\omega^4+\beta_1\omega^2+\beta_0}{7\omega^6+5\alpha_2\omega^4+3\alpha_1\omega^2+\alpha_0}. \tag{23}$$

The coefficients appearing in (22) and (23) are given in the Appendix.

### A. Equal gains

We begin by considering the case where all three modes have equal gains $\gamma_2=\gamma_3=1$. This can be thought of as an approximation for a laser with a very small spread in the modal gains. Equation (22) has the obvious trivial root

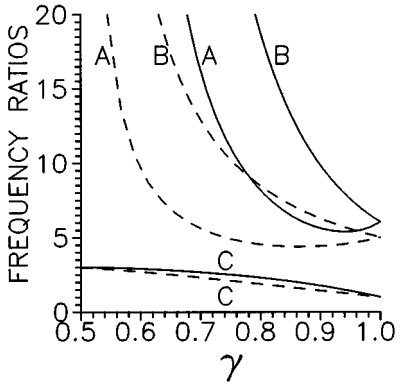


FIG. 2. The ratios $A=(\Omega_R''/\Omega_{L1}'')^2$, $B=(\Omega_R''/\Omega_{L2}'')^2$, and $C=(\Omega_{L1}''/\Omega_{L2}'')^2$ as functions of $\gamma$ for $w-w_3=1$ (solid curves) and for $w\to\infty$ (dashed curves).

$$\omega_1'=0. \tag{24}$$

The other six nonzero roots are easily obtained using the coefficients (A8)–(A10):

$$\omega_{2,3}'=\pm 2\pi i\delta\Omega_R',$$

$$\Omega_R'=\frac{1}{2\pi\delta}\left(\frac{(D^s-1)(5D^s-12)}{5D^s-6}\right)^{1/2}=\frac{1}{2\pi\delta}\sqrt{w-1}, \tag{25}$$

$$\omega_{4,5}'=\omega_{6,7}'=\pm 2\pi i\delta\Omega_L', \quad \Omega_L'=\frac{1}{2\pi\delta}\left(\frac{D^s(1-D^s)}{5D^s-6}\right)^{1/2}. \tag{26}$$

Close to the lasing threshold $w=1$, the low oscillation frequency has the simple scaling

$$\Omega_L'/\Omega_R'=\sqrt{1/7}[1+O(w-1)]. \tag{27}$$

From (23) and (A8)–(A13) we obtain the corresponding real parts

$$\Gamma(\omega_1')\equiv\Gamma_1'=\frac{(5D^s-6)^2+6}{(5D^s-6)(5D^s-12)},$$

$$\Gamma(\omega_{2,3}')\equiv\Gamma_R'=\frac{7[D^s-(D^s-1)(5D^s-6)]}{2(5D^s-6)(5D^s-12)},$$

$$\Gamma(\omega_{4,5}')=\Gamma(\omega_{6,7}')\equiv\Gamma_L'=\frac{D^s}{2(6-5D^s)}.$$

The inequalities (9) and (10) guarantee that all the $\Gamma'$ are positive. The dynamics of these lasers is characterized by oscillations with the frequencies 0, $\Omega_L'$, and $\Omega_R'$ (with $\Omega_L'<\Omega_R'$) that are damped with the corresponding decay rates $\Gamma_1'$, $\Gamma_R'$, and $\Gamma_L'$. A simple relation between $\Omega_R'$ and $\Omega_L'$ is easily derived from (25) and (26):

$$\left(\frac{\Omega_R'}{\Omega_L'}\right)^2=\frac{12}{D^s}-5.$$

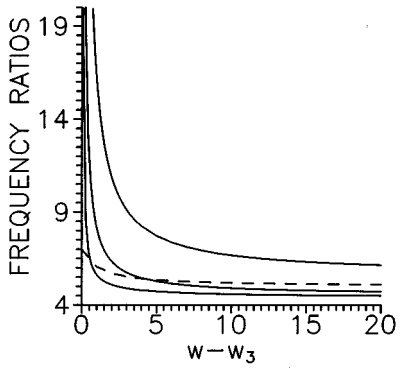


FIG. 3. $(\Omega_R''/\Omega_{L1}'')^2$ versus $w-w_3$ for $\gamma=0.7$, 0.8, 0.9 (full lines from top to bottom) and $\gamma=1$ (dashed line).

Thus this ratio can only vary between 7 for $D^s=1$ (when $w=1$) and 5 for $D^s=6/5$ (when $w=\infty$).

To see the phase coherence between the lasing modes, we derive the eigenvectors corresponding to the seven eigenvalues we have obtained. In the $z$ representation (21) they have the form

$$z_1'=\left\{\frac{1}{2},0,3,0,1,0,1\right\},$$

$$z_{2,3}'=\left\{\frac{3}{5D^s-6}, \frac{\mp 6\pi i\delta\Omega_R'}{5D^s-6},3, \times\frac{\mp 2\pi i\delta\Omega_R'}{5D^s-6},1, \frac{\mp 2\pi\delta\Omega_R'}{5D^s-6},1\right\},$$

$$z_{4,5}'=\left\{0,0,0,0,0, \frac{\pm 2\pi i\delta\Omega_L'}{D^s},1\right\},$$

$$z_{6,7}'=\left\{0,0,0, \frac{\pm 2\pi i\delta\Omega_L'}{D^s},1,0,0\right\}.$$

It is manifest that the modal intensities and population gratings are inphased at frequency $\Omega_R'$ but perfectly antiphased at frequency $\Omega_L'$. The perfect antiphased dynamics at $\Omega_L'$ is reflected in the fact that all the global variables $\mathcal{D}$, $\mathcal{S}$, and $\mathcal{N}$ vanish in $z_{4,5}'$ and $z_{6,7}'$. This is because phase coherence occurs so that the contribution of the modal variables to the global variables cancels out completely at frequency $\Omega_L'$.

### B. Two equal gains

The next case of practical importance is a central mode having the largest gain with two smaller but equal gains for the side modes, i.e., $\gamma_2=\gamma_3=\gamma<1$. The dynamics of such lasers is controlled by both the pump rate $w$ and the gain $\gamma$. In this case the function $f(\omega^2)$ in (22) factorizes

$$f(\omega^2)=(\omega^2+a)(\omega^4+b\omega^2+c), \tag{28}$$

TABLE I. Parameters for which $\Omega_R''=3\Omega_{L1}''$ with $\gamma_2=\gamma_3=\gamma$.

| $\gamma$ | 0.7 | 0.8 | 0.9 |
|---|---|---|---|
| $w-w_3$ | 3.1074 | 0.8156 | 0.2479 |

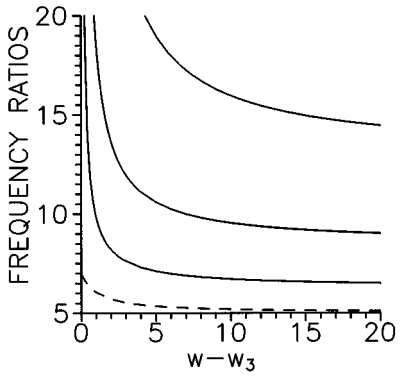


FIG. 4. $(\Omega_R''/\Omega_{L2}'')^2$ versus $w-w_3$ for $\gamma=0.7$, 0.8, 0.9, and 1 (from top to bottom).

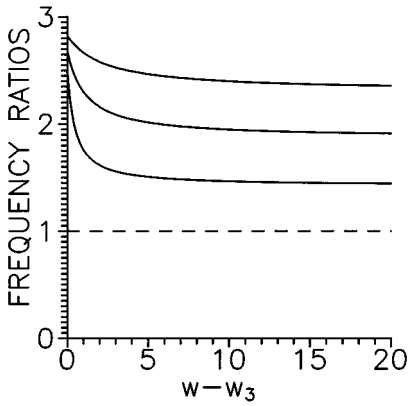


FIG. 5. $(\Omega_{L1}''/\Omega_{L2}'')^2$ versus $w-w_3$ for $\gamma=0.7$, 0.8, 0.9, and 1 (from top to bottom).

where

$$a=\gamma D^s(1-\gamma D^s)/M,$$

$$b=[8+4\gamma-16\gamma D^s+\gamma(D^s)^2+3\gamma^2(D^s)^2]/M,$$

$$c=(1-D^s)(\gamma D^s-1)[8-16\gamma-8\gamma D^s+8\gamma^2-4\gamma^2 D^s+5\gamma^2(D^s)^2]/M^2,$$

with

$$M=5\gamma D^s-2\gamma-4. \tag{29}$$

It follows from (9) and (10) that all the coefficients $a$, $b$, and $c$ as well as the discriminant of the quadratic in (28) are positive in the whole range of allowed $\gamma$ and $w$. The six nonzero roots of (22) are

$$\omega_{2,3}''=\pm 2\pi i\delta\Omega_R'', \quad \Omega_R''=\frac{1}{2\pi\delta}\left(\frac{b+\sqrt{b^2-4c}}{2}\right)^{1/2}, \tag{30}$$

$$\omega_{4,5}''=\pm 2\pi i\delta\Omega_{L1}'', \quad \Omega_{L1}''=\frac{1}{2\pi\delta}\left(\frac{b-\sqrt{b^2-4c}}{2}\right)^{1/2}, \tag{31}$$

$$\omega_{6,7}''=\pm 2\pi i\delta\Omega_{L2}'', \quad \Omega_{L2}''=\frac{1}{2\pi\delta}\sqrt{a}. \tag{32}$$

The double prime refers to the case $\gamma_2=\gamma_3=\gamma<1$. It is worth noticing that, in the limit $\gamma\to 1$, $\Omega_R''\to\Omega_R'$ and $\Omega_{L1}''\to\Omega_{L2}''\to\Omega_L'$, reducing to the case of equal gains, as should be. In general, for $\gamma<1$, the three frequencies given in (30)–(32) are different and the inequalities $\Omega_R''>\Omega_{L1}''>\Omega_{L2}''$ hold. Close to the lasing threshold for three modes, the low oscillation frequencies are given by

$$2\pi\delta\Omega_{L1}''=f(\gamma)\sqrt{w-w_3}[1+O(w-w_3)], \tag{33}$$

$$2\pi\delta\Omega_{L2}''=g(\gamma)\sqrt{w-w_3}[1+O(w-w_3)], \tag{34}$$

where $f\geq 0$ and $df/d\gamma<0$ while $g\geq 0$ and $dg/d\gamma>0$ in the relevant range (19) and (20). In the same domain ($w$ close to $w_c$) we find for $\Omega_R''$ the expansion

$$(2\pi\delta\Omega_R'')^2=(w-1)h(\gamma)+O(1),$$

$$h(\gamma)=(2+\gamma+A)/5, \tag{35}$$

$$A^2=(8-84\gamma+147\gamma^2-86\gamma^3+3\gamma^4)/(2-8\gamma+3\gamma^2).$$

To explore new features, we recall that if $\gamma=1$ the ratio $(\Omega_R'/\Omega_L')^2$ varies between 7 and 5 for $w$ increasing from 1 to infinity. However, if $\gamma<1$ the ratios between the various frequencies may vary in a much larger range. The ratios $A=(\Omega_R''/\Omega_{L1}'')^2$, $B=(\Omega_R''/\Omega_{L2}'')^2$, and $C=(\Omega_{L1}''/\Omega_{L2}'')^2$ are plotted in Fig. 2 as functions of $\gamma$ for $w-w_3=1$ (solid curves) and for $w\to\infty$ (dashed curves). For $\gamma\to 1$ we have $C\to 1$; in addition, $A\to B\to 5$ for $w\to\infty$ while $A\to B\to 7$ for $w\to 1$. For $\gamma<1$, $C$ is slightly greater than 1 but $A$ and $B$ can be made arbitrarily large by decreasing $\gamma$, as appears in Fig. 2. In Fig. 3 we draw $(\Omega_R''/\Omega_{L1}'')^2$ versus $w-w_3$ for different $\gamma$. For $\gamma=1$, the ratio $(\Omega_R''/\Omega_{L1}'')^2$ can vary only between 7 and 5 (dashed line). For $\gamma<1$ the range in which $(\Omega_R''/\Omega_{L1}'')^2$ varies is much wider and the value of $(\Omega_R''/\Omega_{L1}'')^2$ can be chosen by selecting appropriate values of $w$ and $\gamma$. For instance, we find that $(\Omega_R''/\Omega_{L1}'')^2=9$ for the parameters listed in Table I. When $\Omega_R''=3\Omega_{L1}''$ one may expect in experiments with external modulations a resonant effect such as a small amplitude modulation at $\Omega_{L1}''$ leading to a large amplitude change at $\Omega_R''$ due to third harmonic generation. Similar curves for $(\Omega_R''/\Omega_{L2}'')^2$ and $(\Omega_{L1}''/\Omega_{L2}'')^2$ are plotted in Figs. 4 and 5, respectively. We find, for instance, that $\Omega_R''=3\Omega_{L2}''$ for $(\gamma, w-w_3)=(0.9, 1.3563)$ and $\Omega_R''=4\Omega_{L2}''$ for the parameters listed in Table II. For these pairs of pump and gain, a large amplitude response at $\Omega_R''$ may be induced by a small amplitude periodic modulation at the lower frequency via harmonic generation. Let us emphasize that this kind of resonant response does not happen for $\gamma=1$ and hence is specific for the laser with nonequal gains.

This analysis is easily completed by deriving the eigenvectors associated with the eigenvalues (30)–(32). They are given by

$$z_1''\equiv z_1', \tag{36}$$

$$z_{2,3}''=\left\{\frac{3}{M},\ \frac{\mp 6\pi i\delta\Omega_R''}{M},\ \frac{3}{\mu_R}[(\gamma D^s-1)(4-4\gamma+\gamma D^s)+M(2\pi\delta\Omega_R'')^2],\ \frac{\mp 12\pi i\delta\Omega_R''}{M\mu_R}(\gamma D^s-1)(\gamma D^s-\gamma-1),\right.$$
$$\frac{6(1-\gamma D^s)}{M\mu_R}[4-4\gamma-4\gamma D^s+3(\gamma D^s)^2-M(2\pi\delta\Omega_R'')^2],\ \frac{\mp 12\pi i\delta\Omega_R''}{M\mu_R}(\gamma D^s-1)(\gamma D^s-\gamma-1),$$
$$\left.\frac{6(1-\gamma D^s)}{M\mu_R}[4-4\gamma-4\gamma D^s+3\gamma^2 D^s-M(2\pi\delta\Omega_R'')^2]\right\}, \tag{37}$$

$$z_{4,5}''=\{(\text{same as } z_{2,3}'' \text{ with subscript } R \text{ replaced by } L1)\}, \tag{38}$$

$$z_{6,7}''=\left\{0,0,0,\ \frac{\mp 2\pi i\delta\Omega_{L2}''}{\gamma D^s},-1,\ \frac{\pm 2\pi i\delta\Omega_{L2}''}{\gamma D^s},1\right\}, \tag{39}$$

where $M$ is defined by (29) and $\mu_\nu$ with $\nu=R$ or $L1$ is defined through

$$\mu_\nu=(1-\gamma D^s)(4-4\gamma-4\gamma D^s+3\gamma^2 D^s)+\gamma M(2\pi\delta\Omega_\nu'')^2.$$

The intensity phase coherence at one given frequency is characterized by comparing the corresponding components of each of the eigenvectors (37)–(39). Let $P_p(\Omega)$ and $P_T(\Omega)$ be the peak height at frequency $\Omega$ in the power spectra of the modal and total intensities, respectively. Then, from (37)–(39) it immediately follows that

$$\frac{P_T(\Omega_R'')}{P_1(\Omega_R'')}=\frac{\mu_R^2}{\gamma^2[(\gamma D^s-1)(8-3\gamma D^s)+M(2\pi\delta\Omega_R'')^2]^2}, \tag{40}$$

$$\frac{P_1(\Omega_R'')}{P_2(\Omega_R'')}=\frac{P_1(\Omega_R'')}{P_3(\Omega_R'')}=\frac{\gamma^2[(\gamma D^s-1)(8-3\gamma D^s)+M(2\pi\delta\Omega_R'')^2]^2}{4(\gamma D^s-1)^2(\gamma D^s-\gamma-1)^2}, \tag{41}$$

$$\frac{P_T(\Omega_{L1}'')}{P_2(\Omega_{L1}'')}=\frac{P_T(\Omega_{L1}'')}{P_3(\Omega_{L1}'')}=\frac{\mu_{L1}^2}{4(\gamma D^s-1)^2(\gamma D^s-\gamma-1)^2}, \tag{42}$$

$$\frac{P_1(\Omega_{L1}'')}{P_2(\Omega_{L1}'')}=\frac{P_1(\Omega_{L1}'')}{P_3(\Omega_{L1}'')}=\frac{\gamma^2[(\gamma D^s-1)(8-3\gamma D^s)+M(2\pi\delta\Omega_{L1}'')^2]^2}{4(\gamma D^s-1)^2(\gamma D^s-\gamma-1)^2}. \tag{43}$$

TABLE II. Parameters for which $\Omega_R''=4\Omega_{L2}''$ with $\gamma_2=\gamma_3=\gamma$.

| $\gamma$ | 0.7 | 0.8 | 0.9 |
|---|---|---|---|
| $w-w_3$ | 9.8496 | 1.3741 | 0.3361 |

In Fig. 6 we plot $P_T(\Omega_R'')/P_1(\Omega_R'')$ and $P_1(\Omega_R'')/P_2(\Omega_R'')$ as a function of $\gamma$ for different $w$. When $\gamma\to 1$ we have $P_T(\Omega_R'')\to 9P_1(\Omega_R'')=9P_2(\Omega_R'')=9P_3(\Omega_R'')$ but for $\gamma<1$ the following relations hold:

$$P_T(\Omega_R'')>P_1(\Omega_R'')>P_2(\Omega_R'')=P_3(\Omega_R''). \tag{44}$$

Figure 7 is similar to Fig. 6 but for $P_T(\Omega_{L1}'')/P_2(\Omega_{L1}'')$ and $P_1(\Omega_{L1}'')/P_2(\Omega_{L1}'')$ for which the following relations hold:

$$P_T(\Omega_{L1}'')<P_2(\Omega_{L1}'')=P_3(\Omega_{L1}'')<P_1(\Omega_{L1}''). \tag{45}$$

The relations (44) and (45) indicate that the intensity phase coherence occurs differently at $\Omega_R''$ and $\Omega_{L1}''$. It can be verified that in $z_{2,3}''$ the components $\mathbb{l}_1$, $\mathbb{l}_2$, and $\mathbb{l}_3$ have the same sign, implying an inphased coherence. This is why the peak of the total intensity is largest at $\Omega_R''$, as implied by the relations (44). On the other hand, in $z_{4,5}''$ the sign of the component $\mathbb{l}_1$ is opposite to the sign of $\mathbb{l}_2$ and $\mathbb{l}_3$, implying an antiphased coherence at $\Omega_{L1}''$.

A complementary expression of these properties is obtained by seeking relations among the power spectra peaks in the form found in [16]. From the explicit form of the eigenvectors (37)–(39), the following relations are easily established:

$$\Omega=\Omega_R'':\quad P_T=(\sqrt{P_2}+\sqrt{P_3}+\sqrt{P_1})^2,$$

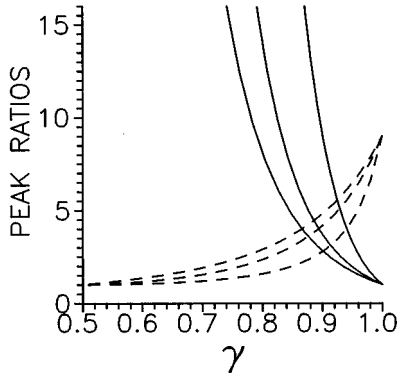


FIG. 6. The dashed lines represent the ratio $P_T(\Omega_R'')/P_1(\Omega_R'')$ as a function of $\gamma$ for $w-w_3=1$, 5, and $\infty$ from bottom to top. The full lines represent the ratio $P_1(\Omega_R'')/P_2(\Omega_R'')=P_1(\Omega_R'')/P_3(\Omega_R'')$ as a function of $\gamma$ for $w-w_3=1$, 5, and $\infty$ from right to left.

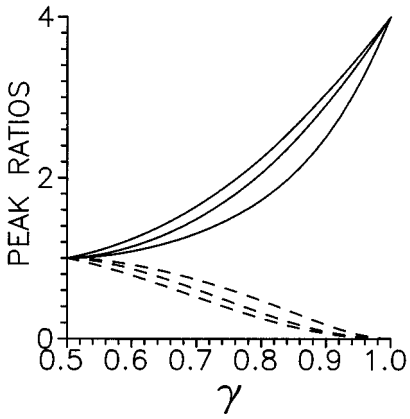


FIG. 7. The dashed lines represent $P_T(\Omega''_{L1})/P_2(\Omega''_{L1})$ as a function of $\gamma$ for $w-w_3=1$, 5, and $\infty$ from top to bottom. The full lines represent the ratio $P_1(\Omega''_{L1})/P_2(\Omega''_{L1})=P_1(\Omega''_{L1})/P_3(\Omega''_{L1})$ as a function of $\gamma$ for $w-w_3=1$, 5, and $\infty$ from bottom to top.

$$\text{with} \quad P_2=P_3\neq P_1, \tag{46}$$

$$\Omega=\Omega''_{L1}: \quad P_T=(\sqrt{P_2}+\sqrt{P_3}-\sqrt{P_1})^2,$$

$$\text{with} \quad P_2=P_3\neq P_1, \tag{47}$$

$$\Omega=\Omega''_{L2}: \quad P_T=(\sqrt{P_2}-\sqrt{P_3}+\sqrt{P_1})^2,$$

$$\text{with} \quad P_2=P_3, \quad P_1=0. \tag{48}$$

The only vanishing peak height in these three relations is $P_1$ at $\Omega''_{L2}$.

The degree of antiphase at frequency $\Omega''_{L1}$ can be characterized by the function defined as

$$\chi(\Omega''_{L1})=1-\frac{P_T(\Omega''_{L1})}{\left(\sum_p \sqrt{P_p(\Omega''_{L1})}\right)^2}. \tag{49}$$

The value $\chi=1$ corresponds to 100%, i.e., perfect, antiphase: there is no peak in the power spectrum of the total intensity of the peak at $\Omega''_{L1}$. An inphased coherence between the modes corresponds to $\chi=0$. In Fig. 8 we draw $\chi(\Omega''_{L1})$ as a function of $\gamma$ for several values of $w$. For $\gamma\to 1/2$ the antiphase degree approaches asymptotically its minimum

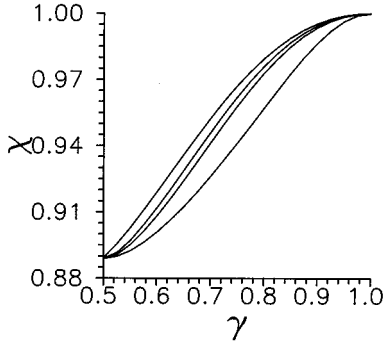


FIG. 8. Degree of antiphase at $\Omega''_{L1}$ versus $\gamma$ for $w-w_3=1$, 5, 10, and $\infty$ (from bottom to top).

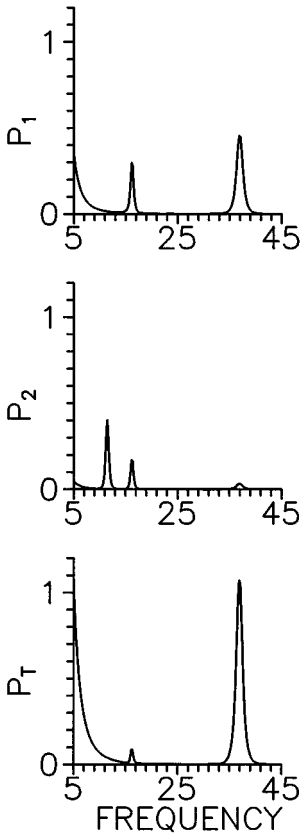


FIG. 9. Power spectra of mode 1 intensity ($P_1$), mode 2 intensity ($P_2$), and the total intensity ($P_T$) obtained by solving numerically the Tang, Statz, and deMars equations for $k=10^4$, $\gamma=0.8$, and $w=7$. $P_2$ and $P_3$ have peaks at the same frequencies. The initial condition is $x_j=(1+0.005j^2)x_j^0$ where $x_1=D$, $x_{2,3,4}=D_{1,2,3}$, $x_{5,6,7}=I_{1,2,3}$, and $x_j^0$ is the steady state of $x_j$ for $w=5$.

$\chi_{\min}=8/9$ in which case we have $P_1(\Omega''_{L1})=P_2(\Omega''_{L1})=P_3(\Omega''_{L1})=P_T(\Omega''_{L1})$. In the limit $\gamma\to 1$, the degree of antiphase $\chi\to 1$ and the power spectra peaks tend towards the asymptotic values $P_1(\Omega''_{L1})\to 2P_2(\Omega''_{L1})=2P_3(\Omega''_{L1})$ and $P_T(\Omega''_{L1})\to 0$. The degree of antiphase at $\Omega''_{L1}$ displayed in Fig. 8 increases from 8/9 where the total intensity peak is lowest in accordance with (45). It is also clear that the difference $1-\gamma$ is a measure of the antiphased coherence at this frequency.

To assess quantitatively this analysis we present in Fig. 9 the power spectra obtained from the numerical integration of Eqs. (1)–(3) for $k=10^4$, $\gamma=0.8$, and $w=7$. Besides the qualitative tendency ruled by the relations (44) and (45), our calculated results $\Omega''_R=37.3684$, $\Omega''_{L1}=16.3131$, $\Omega''_{L2}=13.5315$, $P_T(\Omega''_R)/P_1(\Omega''_R)=2.3525$, $P_1(\Omega''_R)/P_2(\Omega''_R)=14.0383$, $P_T(\Omega''_{L1})/P_1(\Omega''_{L1})=0.1556$, and $P_1(\Omega''_{L1})/P_2(\Omega''_{L1})=2.0572$ reproduce very well the numerical results in Fig. 9. We also find that for this numerical simulation the relations (44) and (45) between the peak heights are valid for the whole range of $\gamma$ as shown in Tables III and IV.

As for the intensity phase coherence at frequency $\Omega''_{L2}$ there is perfect antiphasing independent of $\gamma$ because in $z''_{6,7}$ we always have $\mathcal{S}=0$ due to $\mathbb{I}_2=-\mathbb{I}_3$ and $\mathbb{I}_1=0$. This result is again confirmed numerically in Fig. 9, which shows no peak at $\Omega''_{L2}$ in the power spectra of both the total inten-

TABLE III. Calculated and numerical results for the peak height ratios at frequency $\Omega_R''$ for a wide range of $\gamma$. The parameters used are $k=10^4$, $w-w_3=1$, and the initial state is taken as $x_j=(1+0.005j^2)x_j^0$ where $x_1=D$, $x_{2,3,4}=D_{1,2,3}$, $x_{5,6,7}=I_{1,2,3}$, and $x_j^0$ is the steady state of $x_j$ for $w-w_3=0.9$.

| $\gamma$ | $P_T/P_1$ calculated | $P_T/P_1$ numerical | $P_2/P_1$ calculated | $P_2/P_1$ numerical |
|---|---|---|---|---|
| 0.95 | 4.4454 | 4.4657 | 0.3071 | 0.3097 |
| 0.85 | 1.9954 | 1.9983 | 0.0426 | 0.0427 |
| 0.75 | 1.3549 | 1.3631 | 0.0067 | 0.0069 |
| 0.65 | 1.1130 | 1.1163 | 0.0007 | 0.0007 |

sity and mode 1 intensity. In the power spectra of mode 2 and mode 3 intensities there are three peaks with those at $\Omega_{L2}''$ being perfectly antiphased.

## IV. CONCLUSION

The main result of this paper is the proof that the spread of the modal gain distribution induces gain-dependent variations for the relaxation frequencies over a wide range. In this range, it is quite easy to find values of the parameters for which the ratio between the highest frequency $\Omega_R''$ and either of the two lower frequencies $\Omega_{L1}''$ or $\Omega_{L2}''$ is a small integer (typically 2, 3, or 4) at a reasonably low pump rate. It is expected that these rational relations among the relaxation frequencies may be the source of resonance phenomena in multimode lasers.

The perfect antiphase at $\Omega_{L2}''$ is associated with the symmetry brought about by the coincidence of two gains $\gamma_2=\gamma_3=\gamma$. If all gains are different, only partial antiphase is expected at the lower frequencies. The degree of antiphase increases as the gain difference decreases.

Another class of results we have obtained are relations between the power spectra peaks. The relations (44)–(48) for the peak heights are independent of the initial condition, because they relate components of the same eigenvector. They are also independent of the system parameters, though the more complete results (40)–(43) are functions of the system parameters. In this sense, the relations (44)–(48) are universal. The discrepancy between the calculated and numerical results (presented in Tables III and IV) is about 1%, i.e., of the order of $\delta$. The smallness of $\delta$ is thus a necessary condition for the validity of our analytical treatment which is indeed based on the fact that $\delta=1/\sqrt{k}\ll 1$. The other assumption is the linearization that requires small initial deviations from the steady state. The smallness of $\delta$ also means that the period, proportional to $O(\delta)$, of the relaxation oscillation is much shorter than the decay time that scales as $O(1)$. It is the existence of these two widely different time scales that induces the intensity phase coherence which, in turn, leads to the universal relations (44) and (45).

TABLE IV. Same as in Table I but at frequency $\Omega_{L1}''$.

| $\gamma$ | $P_T/P_2$ calculated | $P_T/P_2$ numerical | $P_1/P_2$ calculated | $P_1/P_2$ numerical |
|---|---|---|---|---|
| 0.95 | 0.0510 | 0.0403 | 3.1478 | 3.1770 |
| 0.85 | 0.3228 | 0.3371 | 2.0502 | 2.0877 |
| 0.75 | 0.6107 | 0.5834 | 1.4848 | 1.5427 |
| 0.65 | 0.8352 | 0.8464 | 1.1796 | 1.2253 |

## ACKNOWLEDGMENTS

This work was supported in part by the Fonds de la Recherche Scientifique and the Interuniversity Attraction Pole program of the Belgian government.

## APPENDIX

The coefficients appearing in Eqs. (22) and (23) are

$$\alpha_0=\frac{D^s(\gamma_1D^s-1)(\gamma_2D^s-1)(\gamma_3D^s-1)[5(D^s)^2-4S_1D^s+8(S_2-S_3)]}{(5D^s-2S_1)^3}, \tag{A1}$$

$$\alpha_1=\frac{-3S_7(D^s)^4+14S_6(D^s)^3-(8S_5+9)(D^s)^2+4S_4D^s+8(S_3-S_2)}{(5D^s-2S_1)^2}, \tag{A2}$$

$$\alpha_2=\frac{S_6(D^s)^2-15D^s+4S_1}{5D^s-2S_1}, \tag{A3}$$

$$\beta_0=\frac{(D^s)^2(\gamma_1D^s-1)(\gamma_2D^s-1)(\gamma_3D^s-1)[25(D^s)^2-20S_1D^s+2(8S_3-S_2)]}{(5D^s-2S_1)^4}, \tag{A4}$$

$$\beta_1=\frac{2D^s}{(5D^s-2S_1)^3}[-7S_7(D^s)^4+2(11S_6+4S_9)(D^s)^3-(4S_8+11S_5+81)(D^s)^2+(3S_4+38S_2)D^s-2(S_2+6S_3)], \tag{A5}$$

$$\beta_2=\frac{7S_6(D^s)^3-(8S_5+9)(D^s)^2+2(2S_4+9S_1)D^s-14S_2}{(5D^s-2S_1)^2}. \tag{A6}$$

Among the gain-dependent sums $S_n$, the sums $S_1$ and $S_2$ are defined in (8) and (11) whereas $S_3$, $S_4$,..., $S_8$ and $S_9$ are given by

$$S_3=\frac{1}{2}\sum_{p,q}{}' \frac{1}{\gamma_p\gamma_q},\quad S_4=\sum_{p,q}{}' \frac{\gamma_p}{\gamma_q^2},\quad S_5=\sum_{p,q}{}' \frac{\gamma_p}{\gamma_q},$$

$$S_6=\sum_{p}\gamma_p,\quad S_7=\frac{1}{2}\sum_{p,q}{}'\gamma_p\gamma_q,\quad S_8=\frac{1}{2}\sum_{p,q,l}{}' \frac{\gamma_p\gamma_q}{\gamma_1^2},$$

$$\text{and}\quad S_9=\frac{1}{2}\sum_{p,q,l}{}' \frac{\gamma_p\gamma_q}{\gamma_l}, \tag{A7}$$

where the prime means $p\neq q$ in double sums and $p\neq q\neq l\neq p$ in triple sums.

### Equal gains

When all gains are equal, the coefficients take the simpler form

$$\alpha_0'=\frac{(D^s)^2(D^s-1)^3(5D^s-12)}{(5D^s-6)^3}, \tag{A8}$$

$$\alpha_1'=\frac{3D^s(8-3D^s)(D^s-1)^2}{(5D^s-6)^2}, \tag{A9}$$

$$\alpha_2'=\frac{3(D^s)^2-15D^s+12}{5D^s-6}, \tag{A10}$$

$$\beta_0'=\frac{(D^s)^2(D^s-1)^3[25(D^s)^2-60D^s+42]}{(5D^s-6)^4}, \tag{A11}$$

$$\beta_1'=\frac{2D^s[-21(D^s)^4+90(D^s)^3-159(D^s)^2+132D^s-42]}{(5D^s-6)^3}, \tag{A12}$$

$$\beta_2'=\frac{21(D^s)^3-57(D^s)^2+78D^s-42}{(5D^s-6)^2}. \tag{A13}$$


[1] K. Wiesenfeld, C. Bracikowski, G. James, and R. Roy, Phys. Rev. Lett. **65**, 1748 (1990).

[2] P. Le Boudec, C. Jaouen, P. L. François, J.-F. Bayon, F. Sanchez, P. Besnard, and G. Stephan, Opt. Lett. **18**, 1890 (1993).

[3] P. Mandel and J.-Y. Wang, Opt. Lett. **19**, 533 (1994).

[4] J.-Y. Wang and P. Mandel, Phys. Rev. A **48**, 671 (1993); J.-Y. Wang, P. Mandel, and T. Erneux, Quantum Semiclass. Opt. **7**, 169 (1995); J.-Y. Wang and P. Mandel, Phys. Rev. A **52**, 1474 (1995).

[5] K. Otsuka, Phys. Rev. Lett. **67**, 1090 (1991).

[6] B. A. Nguyen and P. Mandel, Opt. Commun. **112**, 235 (1994).

[7] K. Otsuka, M. Georgiou, and P. Mandel, Jpn. J. Appl. Phys. **31**, L1250 (1992).

[8] K. Otsuka, P. Mandel, S. Bielawski, D. Derozier, and P. Glorieux, Phys. Rev. A **46**, 1692 (1992).

[9] S. Bielawski, D. Derozier, and P. Glorieux, Phys. Rev. A **46**, 2811 (1992).

[10] P. Mandel, M. Georgio, K. Otsuka, and D. Pieroux, Opt. Commun. **100**, 341 (1993).

[11] K. Otsuka, P. Mandel, M. Georgiou, and C. Etrich, Jpn. J. Appl. Phys. **32**, L318 (1993).

[12] E. A. Viktorov, D. R. Klemer, and M. A. Karim, Opt. Commun. **113**, 441 (1995).

[13] N. B. Abraham, L. L. Everett, C. Iwata, and M. B. Janicki, Proc. SPIE Int. Soc. Opt. Eng. **2095**, 16 (1994).

[14] D. Pieroux and P. Mandel, Opt. Commun. **107**, 245 (1994).

[15] C. L. Tang, H. Statz, and G. deMars, J. Appl. Phys. **34**, 2289 (1963).

[16] P. Mandel and J.-Y. Wang, Phys. Rev. Lett. **75**, 1923 (1995).

[17] D. Pieroux, T. Erneux, and P. Mandel (unpublished).

[18] P. A. Khandokhin, P. Mandel, I. V. Koryukin, B. A. Nguyen, and Ya. I. Khanin (unpublished).